ELSEVIER

Inspection of specular and painted surfaces with centralized fusion techniques

F. Puente León [a,*], S. Kammel [b]

[a] *Technische Universität München, Lehrstuhl für Messsystem- und Sensortechnik, D-80290 Munich, Germany*
[b] *Universität Karlsruhe (TH), Institut für Mess- und Regelungstechnik, Postfach 6980, D-76128 Karlsruhe, Germany*

Abstract

This contribution presents new strategies to inspect specular and painted surfaces. Structures on such surfaces are normally only visible, if patterns of the environment are reflected in them. Thus, conventional approaches only yield a little information gain from a single measurement. In our approach, different intensity patterns are systematically generated in the environment of the surface such that these are reflected in the surface and captured by a camera. Following, the recorded images are processed simultaneously by a centralized fusion technique. Since the fused information is closer to the source, a better exploitation of the raw data is achieved. The fusion problem is formulated with an energy function. Its minimization yields the desired surface defects. The methodology is illustrated with two case studies: the analysis of machined surfaces, and the inspection of painted free-form surfaces. In both cases, a reliable yet cost-efficient inspection is attained matching the needs of industry.
© 2005 Elsevier Ltd. All rights reserved.

Keywords: Automated visual inspection; Image fusion; Bayesian fusion theory; Specular surfaces; Illumination; Painted surfaces; Car body parts; Machined surfaces; Smooth surfaces; Structured surfaces

1. Introduction

Automated visual inspection tasks are often concerned with surfaces showing a partly or even perfectly specular behavior. Examples are lenses, car body parts, perfume flacons, machined surfaces, painted surfaces, dies and molds, and, of course, mirrors. However, methods enabling an automated inspection of such surfaces featuring a sufficient accuracy, reliability, and speed are still lacking. Triangulation methods (projection, structured lighting, and shadow techniques) and shape from shading approaches are difficult to use, because they presuppose a diffuse reflectance of the surface [1]. Additionally, these methods feature an insufficient sensitivity regarding small variations of the surface curvature with respect to the demands of automotive industry. Stylus instruments and optical autofocus scanners provide highly accurate measurements that allow a quantitative characterization of defects but are too slow to be utilized in

---
* Corresponding author. Tel.: +49 89289 23350; fax: +49 89289 23348.
E-mail addresses: f.puente@ei.tum.de (F. Puente León), kammel@mrt.uka.de (S. Kammel).

production lines [2]. Interferometric techniques are too sensitive to rough industrial environments, though such methods are successfully being used for the inspection of a variety of optical components [3]. For all of these reasons, inspection of aesthetic surfaces is mostly done manually up to now. The image fusion strategies described in this paper enable one to automate common inspection tasks of a wide variety of surfaces in a robust manner.

In the scope of this paper, we will assume that the surface $\mathbf{s}(\boldsymbol{\xi})$ to be inspected consists of two spatially varying components that contribute to the image intensities measured by the camera of the automated inspection system in a different way [4]:

$$\mathbf{s}(\boldsymbol{\xi}) := \begin{pmatrix} \rho(\theta_i, \varphi_i, \theta_o, \varphi_o, \boldsymbol{\xi}) \\ \zeta(\boldsymbol{\xi}) \end{pmatrix}, \qquad (1)$$

where $\boldsymbol{\xi} := (\xi, \eta)^T$ denotes the lateral world coordinates. The first component of $\mathbf{s}(\boldsymbol{\xi})$,

$$\rho(\theta_i, \varphi_i, \theta_o, \varphi_o, \boldsymbol{\xi}) = \frac{dL_o(\theta_o, \varphi_o, \boldsymbol{\xi}; E_i)}{dE_i(\theta_i, \varphi_i, \boldsymbol{\xi})}, \qquad (2)$$

is the bidirectional reflectance distribution function [5] (BRDF), where the indices "i" and "o" indicate "incident" and "observed," respectively. The BRDF describes the local optical properties of the surface material. In a nutshell, it tells how bright a surface element viewed from the θ_o, φ_o direction will appear, if it is illuminated from the θ_i, φ_i direction. Mathematically, the BRDF is defined as the ratio of radiance dL_o observed in the θ_o, φ_o direction and caused by E_i to the irradiance dE_i caused by an incident flux in the θ_i, φ_i direction. The elevation angle θ and the azimuth φ belong to a local spherical coordinate system with a polar axis parallel to the normal vector $\mathbf{n}_s(\boldsymbol{\xi})$ of the surface. Since we are dealing with (at least partly) specular surfaces, additional information is available on this component. Provided that the surface shows no local defects, we will assume that this component is spatially constant. Consequently, all deviations of this behavior will be assumed to originate from defects that are to be detected.

The second component of $\mathbf{s}(\boldsymbol{\xi})$ is defined as that part of the surface relief which can be resolved by the image acquisition system, that is the macrostructure. Note that the 3-D microstructure, which cannot be spatially resolved, contributes to the BRDF. Here, $\zeta(\boldsymbol{\xi})$ represents the height of the macrostructure of the surface at the lateral location $\boldsymbol{\xi}$.

The vector $\mathbf{s}(\boldsymbol{\xi})$ provides a comprehensive description of the optically relevant properties of the surface. However, in practice it is usually impossible to determine both components of $\mathbf{s}(\boldsymbol{\xi})$ sufficiently fast and at an acceptable expense to accomplish the inspection. Instead, mostly images of the surface are utilized, although some information contained in $\mathbf{s}(\boldsymbol{\xi})$ is lost in the imaging process.

A common problem in the context of imaging of specular surfaces relates to illumination. Perfectly specular surfaces only reflect the light along a specific path such that the angle of the incident light equals the angle of the reflected light. Consequently, if the camera cannot see an illuminated object (typically the light source itself) reflected in the surface, the corresponding image will appear dark, so that only a little information gain will be achieved from that measurement. A possible solution to this problem consists in recording several images with different lighting (or in a different environment). Typically, the information of interest is extracted from each image separately and is then combined at a decision level. As will be demonstrated in the following, a more powerful approach is to process all images simultaneously by means of a centralized fusion strategy.

The remainder of the paper is organized as follows. In the next section, a classification of specular surfaces into structured and smooth surfaces is introduced, and suitable strategies are presented to inspect both types of surfaces, no matter whether their specularity is perfect or only partial. After a short introduction to energy minimization methods, Section 3 describes specific algorithms to accomplish the fusion of the raw images. In Section 4, experimental results demonstrate the good performance of our strategy based on two case studies: the analysis of machined surfaces, and the inspection of painted free-form surfaces. Finally, in Section 5 the fusion methods are applied to a system that enables one to inspect painted surfaces interactively.

2. Inspection principle

Depending on the geometry of the surfaces to be inspected, two cases must be distinguished, for they require a completely different inspection approach. Whenever the macrostructure $\zeta(\boldsymbol{\xi})$ of the surface under consideration is a spatially slowly varying signal with low-pass characteristics, we will consider it as a smooth surface. Otherwise, a structured surface will be assumed.

2.1. Structured surfaces

We assume a structured specular surface to be composed of several facets such that a non-negligible part of the incident light is reflected according to the law of reflection, although diffuse spread may also occur. As shown in [6], this assumption holds for a wide range of technical and engineering surfaces.

To provide an accurate recording of the surface structure, in-focus imaging is required. The camera acquires an image of the environment reflected in the different facets of the surface. The structures configuring the environment, however, appear usually blurred due to the limited depth of field of the imaging optics and the optical properties of the surface. This fact enables one to perform a detection of defects of the surface topography by analyzing the intensities measured by the camera for each facet of the surface. Defects concerning the surface microstructure (i.e. the BRDF), such as an unwanted surface roughness, yield variations of the specularity and will normally produce a loss of contrast [7]. To inspect the second component of the surface $\mathbf{s}(\xi)$, i.e. the topography $\zeta(\xi)$, light-field methods are appropriate. To check whether the slope of a particular facet is correct, a bright pattern is to be located in the environment of the surface such that it can be reflected by an intact facet and viewed by the camera. Obviously, a comprehensive inspection based on this procedure presupposes that the patterns to be visualized be programmable via a computer.

Fig. 1(a) shows a possible configuration to inspect structured surfaces. The patterns are displayed on a hemispherical screen. The surface under investigation is located in the center of the hemisphere, where it is viewed by a camera through an opening in the screen. The actual screen is opaque, although in this rendered scheme a transparency has been chosen to permit viewing of the inside. The binary periodic pattern of this example shows two periods in azimuthal direction, and is constant in elevation direction, as depicted in the example shown at the lower right corner of Fig. 4(a). The patterns itself may be varied mechanically, or, as in our case, optically by means of projection techniques.

2.2. Smooth surfaces

Due to the smoothness of this class of surfaces, visual information inference on their shape is not straightforward. An alternative to standard shape inspection approaches, such as fringe projection techniques, is based on the deflectometric measuring approach. Deflectometry exploits the fact that light is reflected at a specular surface according to the law of reflection. A camera observes a pattern displayed on a screen that is reflected by the surface, as shown in Fig. 1(b). In this configuration, the surface becomes a part of the optical system and therefore distorts the recorded pattern [8]. Because the surface is not observed directly, there is a trade-off between the lateral resolution and the sensitivity of the measurement system that is balanced by the position of the focal plane of the camera; see Fig. 2(left). Focussing on the surface would maximize the lateral resolution of the surface being inspected at the expense of a reduced sensitivity of the method. In contrast, focussing on the screen would enable to exploit the highest resolution possible for the pattern, but
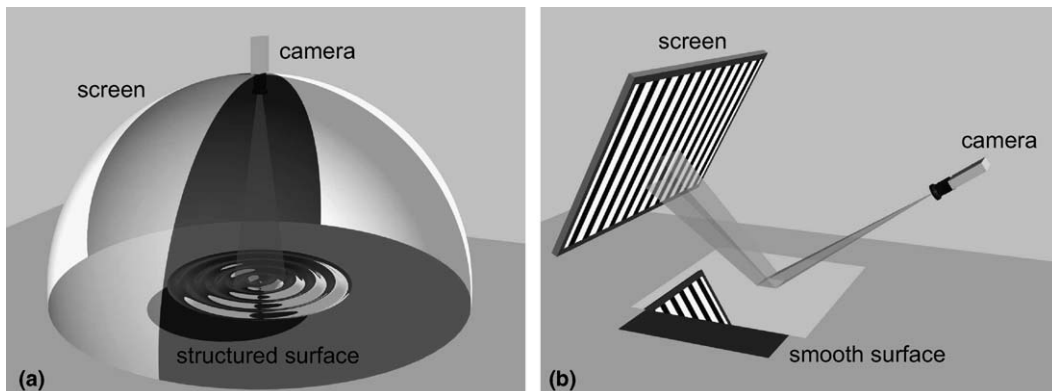
Fig. 1. Setups for inspection of specular surfaces: (a) imaging of structured surfaces; (b) imaging of smooth surfaces.
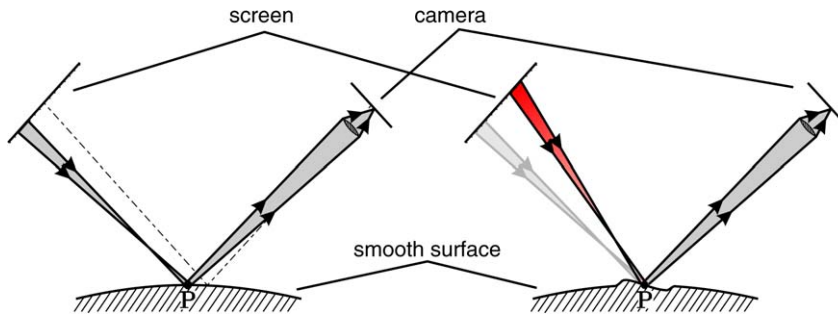
Fig. 2. Measuring principle of deflectometric techniques shown for a flat (left) and a tilted (right) surface. Even a slight change of the local surface slope (right) leads to mapping of a different area of the pattern displayed on the screen.

would also imply a blurring of the surface. If sinusoidal patterns are projected onto the screen, the resolution of the method is limited only by the sensitivity of the image detector, because blurring of such patterns only reduces their contrast.

As shown in Fig. 2(right), this method shows an extremely high sensitivity regarding the local surface slope. Even a slight change of the surface slope leads to mapping of a completely different area of the pattern on the screen. Moreover, the sensitivity of the method can be enhanced by just increasing the distance between the surface and the screen. Thus, this method enables one to detect tiny defects that may be considered aesthetically displeasing, even if they do not entail any functional disadvantage.

3. Fusion

In the scope of this paper, fusion is concerned with the combination of B images

$$\mathscr{D} := \{d(\mathbf{x}, p_i(\boldsymbol{\omega})), \ i = 0, \ldots, B - 1\} \tag{3}$$

to the wanted result $r(\mathbf{x})$, where $\mathscr{P} = \{p_i(\boldsymbol{\omega}), \ i = 0, \ldots, B - 1\}$ represents the set of patterns displayed on the screen, and the magnitude $p_i(\boldsymbol{\omega})$ describes the intensity of the pattern at the location indicated by the vector $\boldsymbol{\omega}$. For both classes of surfaces introduced in the last section, the consideration of two-dimensional patterns has proven to be sufficient to perform the inspection. Consequently, the parameter vector $\boldsymbol{\omega}$ may be expressed in polar coordinates by means of the azimuth ϕ and the elevation angle θ:

$$p_i(\boldsymbol{\omega}) = p_i(\phi, \theta) \quad \text{with } \boldsymbol{\omega} = (\phi, \theta)^{\mathrm{T}}. \tag{4}$$

If the location of a point on the hemispherical screen depicted in Fig. 1(a) is expressed in spherical coordinates (with a constant radius), this representation becomes immediately clear. Although in the

examples presented in Section 4 the result $r(\mathbf{x})$ is a scalar feature image, in other applications one could be interested in obtaining images, symbolic image descriptors, or even a vector containing several results instead; see [9].

The fusion of the sensor data shall take place complementarily. Though the information of interest is distributed over all the images of the series, for a certain location it remains concentrated to a few images. With regards to the fusion strategy to be employed, a centralized approach provides the most robust way to accomplish this task. Since the information fused is closer to the source, a better exploitation of the raw data is achieved [10]. A drawback of such methods is that the resulting algorithms are often ad hoc solutions which in addition tend to be computationally expensive. Thanks to the homogeneity of the sensor data, however, a preprocessing is not needed in the present case. Thus, the computing time can be kept within reasonable limits.

3.1. Fusion approach

The theoretical origins of data fusion date back to the late sixties, although a broad application of these techniques did not took place until the early eighties. In the mean time, the bibliography on data fusion has become very extensive, and applications to several fields have been reported, such as robotics, pattern recognition, medicine, non-destructive testing, geo-sciences, defense, and finances [11]. However, most of the proposed approaches are not systematic, but represent rather ad hoc solutions to specific problems. Some of the few systematic frameworks documented during the last years to perform fusion of image data include statistical approaches (both classical and Bayesian ones),

Dempster–Shafer logical reasoning, fuzzy logic, and neural networks.

A fairly general approach to centralized image fusion consists in expressing all knowledge available a priori on desirable properties and reasonable constraints regarding the raw data $\mathscr{D}$, the nuisance parameters $\mathscr{N}$ [12], and the fusion results $\mathscr{R}$ as well as their interconnections in shape of generalized energy terms $E_k(\mathscr{D}, \mathscr{R}, \mathscr{N})$ [13]. These "energies" E_k have to be chosen such that the knowledge available and the requirements expressed are reflected monotonically in the sense that the result becomes more desirable the lower the energy is. The energy terms are then combined to an energy function E by means of weighted summation:

$$E = \sum_k \lambda_k E_k(\mathscr{D}, \mathscr{R}, \mathscr{N}), \quad \lambda_k > 0. \tag{5}$$

E represents an implicit approach to the fusion task. Due to the monotony of the energy function, the fusion can be accomplished by minimizing E with respect to the fusion results $\mathscr{R}$ and the nuisance parameters $\mathscr{N}$:

$$\{\mathscr{R}^*, \mathscr{N}^*\} = \arg\min_{\mathscr{R}, \mathscr{N}} \{E\}, \tag{6}$$

where $\mathscr{R}^*$ and $\mathscr{N}^*$ denote the results of the optimization.

Some advantages of this approach are its generality as well as the possibility to incorporate additional information and constraints by simply adding further energy terms. Moreover, there is an interesting connection with Bayesian statistics. According to statistical physics, a Gibbs probability density function (PDF) can be defined for the energy function:

$$\mathrm{PDF} \propto \mathrm{e}^{-\frac{E}{T}} = \prod_k \mathrm{e}^{-\lambda_k E_k / T}. \tag{7}$$

T can be thought of as a generalized temperature. Since the energy function is a sum, the PDF can be decomposed into factors. These factors can be interpreted either as a likelihood function or as a priori PDFs. By means of an appropriate normalization of Eq. (7), the a posteriori PDF for the fusion result given the image series is obtained. The monotony of the exponential function ensures that minimizing E is equivalent to maximizing Eq. (7). Therefore, the optimization delivers the maximum a posteriori estimate of the fusion result. It should be emphasized that—since the energy terms do not only embody objective knowledge, but also subjective wishes and requirements—the PDF Eq. (7) is a subjective probability description. However, the advantage of describing fusion from a probabilistic point of view is that there exists a powerful set of mathematical tools for treating Gibbs PDFs. An important example is the simulated annealing optimization method [14].

3.2. Case study 1: Machined surfaces of pressure sensors

The first case study is concerned with the detection of defects on machined surfaces acting as membranes of pressure sensors. The field of inspection is about 10 mm^2, whereas the defects itself are in the order of a few hundredths of a square millimeter. Fig. 3(a) shows an example of such a non-defective surface illuminated with diffuse light, whereas the membrane of Fig. 3(b) features several defects, as can be perceived in the zoomed detail picture on the right. Obviously, these images hardly allow to discern intact regions from defective areas.

To perform the inspection, an image series $\mathscr{D}$ of the surface is recorded by using binary patterns generated according to the following equation:

$$p_i(\theta, \phi) = p_i(\phi) = \frac{1}{2}\left[\mathrm{sgn}\left(\cos\left(2\phi - \frac{2\pi i}{B}\right)\right) + 1\right], \tag{8}$$
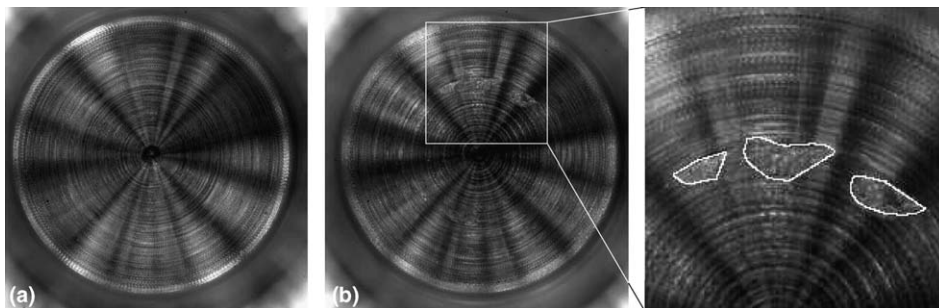
Fig. 3. Machined surfaces of pressure sensors: (a) faultless membrane; (b) defective membrane and zoomed image showing defects.
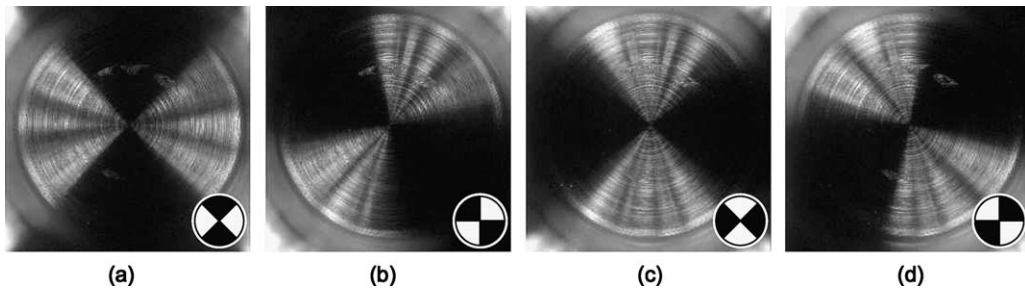
Fig. 4. Images of a membrane of a pressure sensor and corresponding patterns used to record them (lower right corner). (a) $i = 0$; (b) $i = B/4$; (c) $i = B/2$; (d) $i = 3B/4$.

where sgn(.) denotes the signum function:

$$\text{sgn}(x) := \begin{cases} 1 & \text{for } x \geqslant 0 \\ -1 & \text{otherwise} \end{cases}. \tag{9}$$

Fig. 4 shows exemplarily four images out of a series of 16 of a sensor membrane, as well as icons representing the corresponding intensity patterns used to record them. To illustrate the fusion principle, now a certain fixed point $\mathbf{x}$ of the surface shall be considered. If the course of the image intensities at the location $\mathbf{x}$ depending on the image index i is analyzed, a typical signal pattern can be recognized in non-defective regions. Each of the grooves acts as a mirror that reflects the pattern intensities located in both directions perpendicular to their own local direction. Similarly, dark areas should be expected for an intact texture, if the patterns perpendicular to its course are dark. In other words, the local intensity of an ideal groove texture reveals whether the patterns at both sides of it are bright or not. Bright regions emerging from a dark groove texture indicate local defects, as can be seen clearly in Fig. 4(a) and (d). Though this fact would already enable to formulate some detection algorithms based on the analysis of the neighborhood of each pixel, fusion methods provide an enhanced way to detect even tiny surface defects more reliably. No information regarding spatial neighborhoods will be considered, but "neighborhoods" in pattern space will be exploited.

In this particular case, harmonic analysis of the signals $d(\mathbf{x}, p_i)$ enables us to define the following feature image that robustly measures local surface defects:

$$m(\mathbf{x}) := \frac{|D(\mathbf{x}, f_p = 1)|}{|D(\mathbf{x}, f_p = 1)| + |D(\mathbf{x}, f_p = 0)|}, \tag{10}$$

where

$$D(\mathbf{x}, f_p) := \mathscr{F}_p\{d(\mathbf{x}, p_i)\}$$
$$= \sum_{i=0}^{B-1} d(\mathbf{x}, p_i) \cdot \exp\left(-\text{j}2\pi \frac{if_p}{B}\right) \tag{11}$$

denotes the one-dimensional discrete Fourier transform (DFT) of the series with respect to the pattern dimension, that is the index i. Eq. (10) computes a feature based on the comparison of two frequency components of the image intensities at the location $\mathbf{x}$: the fundamental oscillation and the DC component. It is easy to recognize that the resulting values are all within the range $[0, 1]$, and that the ratio 0.5 is obtained when the energy of both components is the same. It is thus straightforward to segment the image into defective and intact regions by choosing a threshold $t = 0.5$.[1] A value higher than t would mean that the fundamental oscillation dominates, i.e. the texture contains no defects at this location. Otherwise, $\mathbf{x}$ is assigned to the set of defective regions.

The resulting energy function is trivial and consists of only one addend:

$$E = \sum_{\mathbf{x}} [r(\mathbf{x}) - m(\mathbf{x})]^2 = E_{\text{feature}}(m(\mathbf{x}), r(\mathbf{x})). \tag{12}$$

Since for the optimal solution $r^*(\mathbf{x}) = m(\mathbf{x})$ holds, a costly minimization is not necessary in this case.

3.3. Case study 2: Painted car body parts

In the second case study, defects on painted car doors are to be detected. Similar to the examination of the membranes of pressure sensors, an image

---

[1] Despite the simplicity of this classification approach, a more robust alternative will be employed in Section 4.

series $\mathscr{D}$ of the surface is recorded using a set of two-dimensional binary patterns

$$p_i(u,v) = \frac{1}{2}\left[\mathrm{sgn}\left(\cos\left(n \cdot \frac{2\pi u}{u_{\max}} - \frac{2\pi i}{B}\right)\right) + 1\right], \quad (13)$$

where $u_{\max}$ denotes the maximum coordinate value in u direction displayable by the device generating the patterns (e.g. the projector), and n is the number of periods to display. For the sake of simplicity, the resulting set of fringe patterns $p_i(u,v)$ has been described in a Cartesian coordinate system (u,v), but is actually projected onto the inside of a hemispherical screen to perform real measurements. According to the law of reflection, a flat screen would restrict the deflectometric measurement system to the inspection of surfaces with a small spread of normal vector directions. The hemispherical shape of the screen, however, allows to view the patterns on the screen after they have been reflected at the surface for the case of most free-form surfaces [15]. Again, the course of the image intensities at a fixed location $\mathbf{x}$ describes a typical signal pattern that enables one to recognize defective regions by means of appropriate analysis techniques.

In addition to defects like scratches, which cause local changes of the BRDF, bubbles and inclusions in the paint or coating should be detected as well. The latter defects are characterized by a much higher curvature as compared with intact surface parts. Therefore, from defective surface areas, the camera receives a compressed view of a large region of the screen. Details of the screen cannot be discriminated from pixels of defective areas, because of the discrete nature of the image formation as well as out-of-focus imaging. Thus, defects are typically imaged with the mean brightness of the visible screen area.

In contrast, image areas that correspond with faultless regions ideally show a sharp image of the screen pattern. To ensure sharp images with high contrast in non-defective areas, it is recommendable to adapt the displayed pattern to the curvature of the surface being examined [16]. Displaying consecutive phase shifted patterns $p_i(u,v)$ results in distinct intensity changes within the areas of the camera image that correspond to faultless surface regions. Defective regions, however, show nearly the same constant grey level. This means that the contrast and thus also the spread of any point $\mathbf{x}$ in the dimension spanned by the pattern index i is high for faultless surface areas and low for defective regions. A suitable measure for the contrast is defined as

$$m_{\mathrm{c}}(\mathbf{x}) := \max_i\{d(\mathbf{x},p_i)\} - \min_i\{d(\mathbf{x},p_i)\}$$

$$\text{with } i = 0, \ldots, B-1. \tag{14}$$

The measure $m_{\mathrm{c}}(\mathbf{x})$ performs well, if the surface being inspected shows a high degree of specularity, and the generated patterns feature a high contrast. On the other hand, this measure is rather susceptible to noise due to its dependence on the extremal values. Thus, for noisy images it is preferable to use other measures, such as the variance

$$m_{\mathrm{v}}(\mathbf{x}) := \frac{1}{B-1}\sum_{i=0}^{B-1}(d(\mathbf{x},p_i) - \bar{d}(\mathbf{x}))^2$$

$$\text{with } \bar{d}(\mathbf{x}) = \frac{1}{B}\sum_{i=0}^{B-1} d(\mathbf{x},p_i). \tag{15}$$

The resulting energy function as well as its optimal solution can be calculated according to Eq. (12).

4. Results

4.1. Structured surfaces

To record the image series of Fig. 4, a commercially available image acquisition system has been used [17]; see Fig. 5(a). It features 768 dimmable light emitting diodes (LED) that allow a flexible, computer-controlled generation of a wide variety of patterns, as shown in the example of Fig. 5(b). The light is incident on a parabolic screen, in the center of which the surface under investigation is located. A CCD camera and a microscope are used to capture the images through an opening in the screen.

Fig. 6 shows the fusion results obtained for both membranes presented in Fig. 3 with the method proposed in Section 3.2. The feature image on the left does not contain any noticeable defects, whereas the image of Fig. 6(b) clearly features several defective areas. The zoomed image on the right of this figure shows an overlay with the results of a further defect detection step. To this end, an edge detection method based on a Laplacian-of-Gaussian (LoG) filter has been used [18].

4.2. Smooth surfaces

For the inspection of car body parts, the setup shown in Fig. 5(c) has been used. This setup consists of an arched screen with a diameter of 1.5 m. A projector with a special fisheye lens is placed in the focal
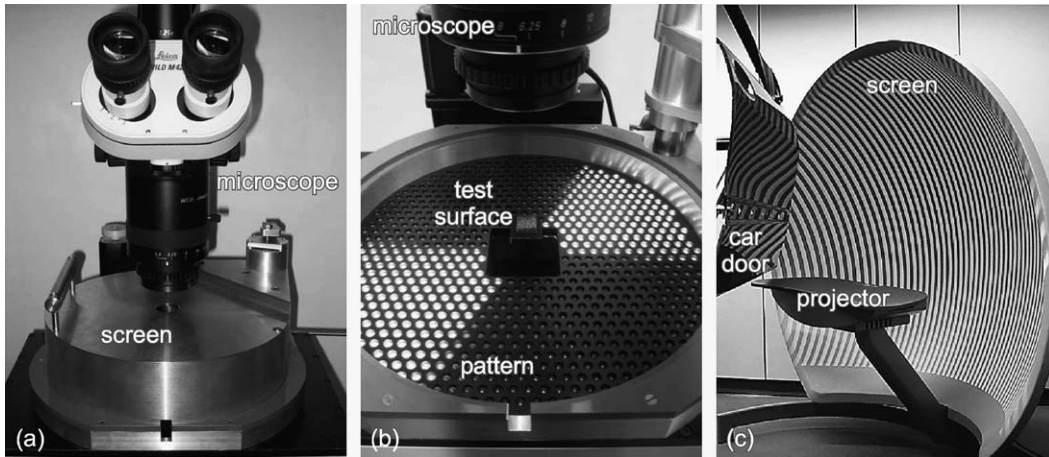
Fig. 5. Image acquisition systems: (a) commercial system GE/2; (b) detail of GE/2 showing a structured test surface and a pattern generated by means of LEDs; (c) setup to inspect car body parts.
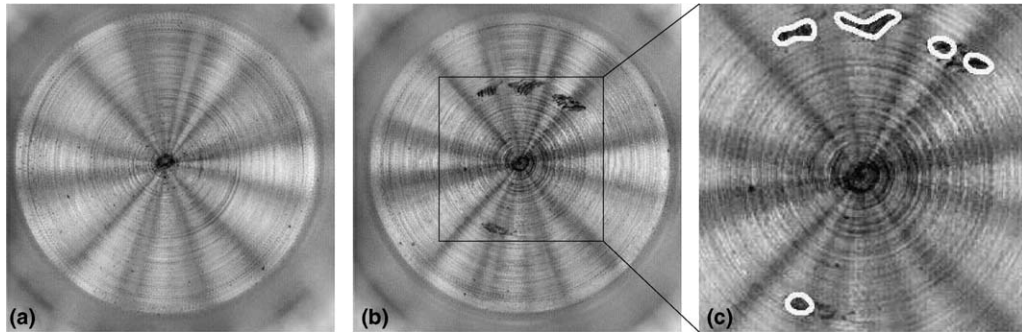
Fig. 6. Fusion results for the membrane of a pressure sensor: (a) resulting feature image for the intact membrane shown in Fig. 3(a); (b) resulting feature image for the defective membrane shown in Fig. 3(b); (c) corresponding detection results.

point of the screen to project arbitrary patterns. The car body part—in this case a car door—is placed above the projector.

First, three different regions on six car doors have been inspected. The car doors constitute a standard set used by a car manufacturer for the evaluation of paint inspection systems. In Fig. 7(a1–a3), three examples of the fusion results for flat regions of these car doors coated with different paints are depicted. The images have been inverted to highlight the faulty regions caused by bubbles and inclusions. The size of the region acquired by the camera is about 25 cm^2. Based on a LoG filtering technique, the fusion results have been segmented and classified into three classes, as demanded by industry standards: tolerable defects (0), removable defects (1), and defects that lead to the rejection of the inspected car body part (3). The lateral dimensions of the found defects are in the range of a few milli-

meters and the depth of the defects ranges from 10 to 200 μm. All defects had been previously classified by the car manufacturer, and with our methods a 100% classification reliability could be achieved (i.e. in all cases the different defects could not only be reliably detected but also assigned to the same class as given by the car manufacturer).

In a second approach, a larger region (about 0.2 m × 0.8 m) of a car door has been inspected using the described fusion technique. Fig. 8 shows the region of the painted car door together with two fusion results. In Fig. 8(a) an image of a region of the inspected car door taken under diffuse lighting is shown. It is almost impossible to perceive any defect with this illumination. In Fig. 8(b), however, the fusion strategy described in Section 3.3 has been applied to images taken while focussing on the screen. This focus setting maximizes the sensitivity of the system at the expense of a low spatial

Fig. 7. Paint defects on flat regions of a car body part: (a1–a3) fusion results; (b1–b3) classification results.
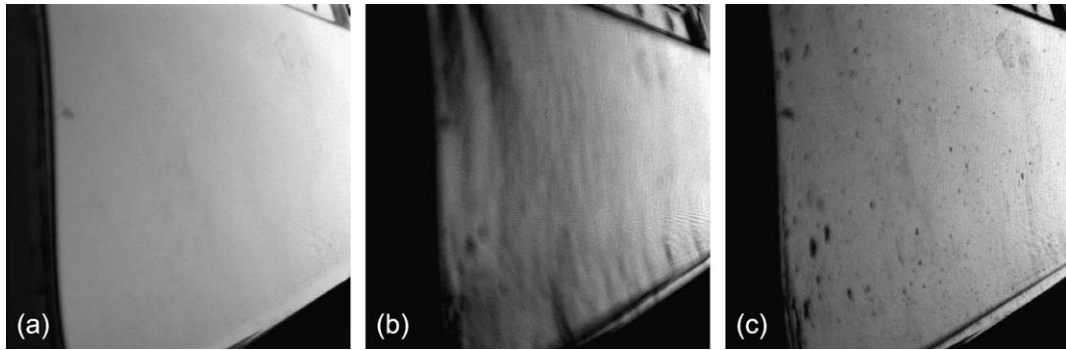
Fig. 8. Images of an area on a car door recorded under diffuse illumination (a) and fusion results for images recorded while focussing on the screen (b) and the door (c).

resolution. The high sensitivity allows to visualize deformations caused by a misadjustment of the forming machine that are nearly invisible to a human observer. Note that in this case the depth of the defects visualized are in the order of magnitude of only a few microns!

In contrast, Fig. 8(c) shows the result of fusing images in which the camera was focussed on the door region directly. With this setting, the resolution is maximized at the expense of a reduced sensitivity. The increased resolution permits a reliable detection of paint defects such as bubbles, inclusions or scratches with a magnitude hardly measurable with alternative methods.

Obviously, since the different focus settings allow to image different spatial frequency components of the surface being inspected, both results complement each other. Together, they provide a much more accurate insight into surface defects as compared with conventional techniques to inspect specular surfaces.

5. Interactive inspection system

A major requisite for a robust in-line inspection of painted surfaces is to combine the reliability of automated systems with the flexibility of human-based techniques to enable an efficient manual refinishing of defective areas. Stepping up to this challenge, we have developed a system that consists of the setup shown in Fig. 5(c), and a mobile inspection device equipped with a head-mounted display (HMD) and a video camera, as shown in Fig. 9(a). The HMD consists of two LC displays to visualize the feature image, as well as a camera used to record the raw data. In Fig. 9(b), the interactive inspection procedure is demonstrated with a car door.
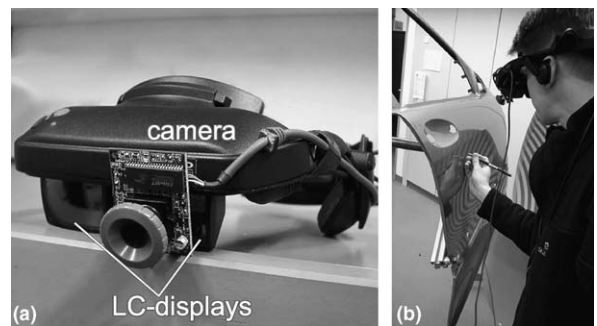
Fig. 9. Head-mounted inspection system: (a) HMD device; (b) interactive inspection procedure is demonstrated with a car door.

During operation, the camera continuously captures images of different fringe patterns reflected in the painted surface, thus emulating the behavior of human examiners. However, before displaying the images in the HMD, they are combined by means of the signal analysis techniques described in Section 3.3 to form an image in which defects appear efficiently enhanced. This way, the information gathered from multiple lighting constellations is concentrated in one single image. Additionally, quantitative detection results can be overlaid to the visualized image to provide an objective assessment.

6. Conclusions

New strategies to inspect specular and painted surfaces have been presented. They are based on image fusion techniques, and feature a very robust behavior in the case of structured as well as smooth surfaces. To record the different images to be fused, complementary imaging conditions are systematically generated by projecting light patterns onto a

screen. To accomplish the fusion, a powerful centralized approach based on energy minimization has been selected. The performance of the presented strategy has been demonstrated by means of two demanding case studies: the analysis of machined surfaces, and the inspection of painted free-form surfaces.

Based on the example of membranes of pressure sensors, a method has been introduced to assess the texture of structured specular surfaces. Conventional methods often yield poor results when applied to such surfaces [19]. The proposed method, however, allows a classification of the discrete image locations point by point, and performs thus very accurately even in the case of defects of only small extent. The second example refers to the inspection of painted surfaces. With the proposed technique, not only scratches, bubbles and inclusions can be detected reliably. Moreover, with the very same setup, also bumps and dents can be visualized just by shifting the focal plane of the camera used. Furthermore, the range of applications of the described methods can easily be extended to diffusely reflecting surfaces, such as unpainted car body parts, by using light of a larger wavelength and recording the corresponding images with an infrared camera.

In both cases, the results show that a reliable yet cost-efficient inspection of specular and painted surfaces is attained matching the needs of industry. The increased expense regarding the acquisition of the image data is more than compensated thanks to a simplified signal processing.

References

[1] B. Denkena, H. Ahlers, F. Berg, T. Wolf, Fast inspection of larger sized curved surfaces by stripe projection, in: Annals of CIRP 51(1), 2002, pp. 499–502.

[2] D.J. Whitehouse, Handbook of Surface Metrology, Institute of Physics Publishing, Philadelphia, 1992.

[3] T. Dresel, G. Häusler, H. Venzke, 3D-sensing with a confocal microscope, Applied Optics 31 (1992) 919–925.

[4] J. Beyerer, F. Puente León, Suppression of inhomogeneities in images of textured surfaces, Optical Engineering 36 (1) (1997) 85–93.

[5] F.E. Nicodemus, J.C. Richmond, J.J. Hsia, I.W. Ginsberg, T. Limperis, Geometrical Considerations and Nomenclature for Reflectance, NBS Monograph 160, National Bureau of Standards, U.S. Department of Commerce, Washington DC, 1977.

[6] P. Kierkegaard, Reflection properties of machined metal surfaces, Optical Engineering 35 (3) (1996) 845–857.

[7] F. Puente León, Enhanced imaging by fusion of illumination series, in: O. Loffeld (Ed.), Sensors, Sensor Systems, and Sensor Data Processing, Proc. SPIE 3100, 1997, pp. 297–308.

[8] D. Pérard, Automated visual inspection of specular surfaces with structured-lighting reflection techniques, Fortschritt-Berichte VDI, Reihe 8, No. 869, VDI Verlag, Düsseldorf, 2001.

[9] F. Puente León, Complementary image fusion for inspection of technical surfaces, Technisches Messen 69 (4) (2002) 161–168 (in German).

[10] D.L. Hall, Mathematical Techniques in Multisensor Data Fusion, Artech House Inc., Norwood, MA, 1992.

[11] X.E. Gros, NDT Data Fusion, Arnold, London, 1997.

[12] J. Beyerer, Is it useful to know a nuisance parameter? Signal Processing 68 (1) (1998) 107–111.

[13] J.J. Clark, A.L. Yuille, Data Fusion for Sensory Information Processing Systems, Kluwer Academic Publishers, Boston, 1990.

[14] S. Kirkpatrick, C.D. Gelatt Jr., M.P. Vecchi, Optimization by simulated annealing, Science 220 (1983) 671–680.

[15] J. Beyerer, D. Pérard, Automatische Inspektion spiegelnder Freiformflächen anhand von Rasterreflexionen, Technisches Messen 64 (10) (1997) 394–400.

[16] S. Kammel, Automated optimization of measurement setups for the inspection of specular surfaces, in: K.G. Harding, J.W.V. Miller (Eds.), Machine Vision and Three-Dimensional Imaging Systems for Inspection and Metrology II, Proc. SPIE 4567, 2002, 199–206.

[17] M. Heizmann, Automated comparison of striation marks with the system GE/2, in: Z.J. Geradts, L.I. Rudin (Eds.), Investigative Image Processing II, Proc. SPIE 4709, 2002, 80–91.

[18] J. Beyerer, F. Puente León, Detection of defects in groove textures of honed surfaces, International Journal of Machine Tools and Manufacture 37 (3) (1997) 371–389.

[19] F. Puente León, Model-based inspection of shot peened surfaces using fusion techniques, in: K.G. Harding, J.W.V. Miller, B.G. Batchelor (Eds.), Machine Vision and Three-Dimensional Imaging Systems for Inspection and Metrology, Proc. SPIE 4189, 2001, 41–52.